A Bipolar electrospray source of singly charged salt clusters of precisely controlled composition

Juan Fernandez de la Mora[b] and César Barrios-Collado [a]
[a] SEADM, Parque tecnológico de Boecillo 205, 47151 Valladolid, SPAIN
[b] Yale University, Mechanical Engineering Department, New Haven, CT 06420-8286

Submitted to Aerosol Science and Technology, October 2016. Revised Jan/26/2017

ABSTRACT

The few clusters $[B^-_nA^+_{n+1}]^+$ (n=0,1) with resolvable mobilities formed in electrosprays of large salts have been used for nanoparticle instrument testing and calibration at sizes smaller than 2 nm. Extensions of this modest size range by charge reduction with uncontrolled gas phase ions has resulted in impure singly charged clusters. Here we combine two oppositely charged electrosprays of solutions of the same salt B^-A^+, including: $(C_nH_{2n+1})_4N^+Br^-$ (n=4,7,12,16), the large phosphonium cation $(C_6H_{13})_3(C_{16}H_{33})P^+$ paired with the anions Im^- [$(CF_3SO_2)_2N^-$] or FAP^- [$(C_2F_5)_3PF_3^-$], and the asymmetric pair [*1-Methyl-3-pentylimidazolium*$^+$*FAP*$^-$]. Both polarities are simultaneously produced by this source in comparable abundances, primarily as singly charged $A^+_nB^-_{n\pm1}$, with tiny contributions from higher charge states. Some but not all of these clusters produce narrow mobility peaks typical of pure ions, even beyond n=43. Excellent independent stable control of the positive and the negative sprays brought very close to each other is achieved by isolating them electrostatically with a symmetrically interposed metallic screen. Two nanoDMAs covering the size range up to 30 nm (Halfmini and Herrmann DMAs, with classification lengths of 2 and 10 cm) are characterized with these standards, revealing resolving powers considerably higher than previously seen with unipolar electrospray sources. The bipolar source of *pure* and chemically homogeneous clusters described permits studying size and charge effects in a variety of aerosol instruments in the 1-4 nm size range.

Running title: Bipolar electrospray source
Key words:

1. Introduction

Monodisperse particle standards have been widely used in aerosol science, particularly in the evaluation of instruments, including differential mobility analyzer (DMA), impactors, condensation particle counters (CPC), etc. So-called monodisperse aerosols, traditionally based on polystyrene spheres or size selection with a DMA, have always had a finite size breadth. Nanometer size standards were traditionally of poor monodispersity, until the development of electrospray (ES) ionization (Fenn et al., 1989) provided them in essentially pure form. Since then, a variety of strictly monodisperse size or mobility standards have become available, permitting unprecedented studies (i.e. Winkler et al. 2012). Molecular mobility standards available by conventional electrospraying, however, have been limited to small sizes (1.7 nm) by the fact that ES produces a complex mixture of clusters appearing in many charge states. As a result, most clusters in this mix cannot be resolved from each other by mobility alone, with the exception of the smallest ones that are singly charged and have peculiarly large mobilities (For some exceptions see Ku and Fernandez de la Mora, 2004, 2009). Charge-reduction of multiply charged electrosprayed clusters has permitted a considerable widening of this range (Kaufman et al., 1996; You et al., 2014; Gamero-Castaño and Fernandez de la Mora, 2000a, b, c; Kaufman and Dorman 2008). The approach, however, reduces the original charge with a mixture of counterions produced by a source of ionizing radiation, and results in approximately monodisperse particles rather than rigorously pure species [Gamero and Fernandez de la Mora (2000a, Figure 7); (2000b, Fig 1b); (2000c, Fig 4c)]. Tandem DMA selection of multiply charged clusters that lose one charge between the two DMAs has increased up to 3.5 nm the available size range (Attoui et al. 2013). However, this method requires two high-resolution DMAs, one of which needs to have a high transmission available only in planar DMAs. Kangasluoma's Thesis (U. Helsinki, 2015; also Kangasluoma et al. 2016) has been especially creative of alternative sources for cluster standards at sizes well beyond those produced by electrospraying salts. Some of these studies have achieved an improved control of the charge reduction process by selecting the counter-ion. This can be performed to a certain degree by exploiting the specificity of certain chemical ionization processes, for instance by resonant laser ionization (Kane et al., 1995, 1996) or by selectively ionizing a species with high ion or electron affinity (Reid et al. 2003). This approach has even been used successfully for the much harder task of producing neutral clusters of selected composition (Steiner et al. 2017). Still, even if an electrospray of $B^-_nA^+_{n+z}$ is charge-reduced by a pure ion C^- (say NO_3^-, which may be selectively created by chemical ionization; Jiang et al. 2011), mixed species of the form $B^-_nA^+_mC^-_{m-n\pm l}$ result. The double degree of freedom *m, n* available, then rapidly scrambles the mobility spectrum even at relatively small sizes, similarly as in the two-parameter space *n, z* spanned by naturally charged electrosprays. A simple solution to this problem is to choose the charge-reducing agent to be either A^+ or B^-. This selective charge-reduction process requires a special counter-ion source, being accordingly complex, and limiting the possibilities to freely vary the anion or the cation.

A considerably simpler source of clusters with only one degree of freedom would be the combination of a positive and a negative electrospray of one given salt. Several variants of the bipolar electrospray have been tried, going back at least to the studies of Borra et al. (1999), and others reviewed recently by Tang (2016). One difficulty encountered is in stabilizing two neighboring oppositely charged electrospray sources, due to counter-ions

in the gas (Tang and Gomez 1995, Lenggoro et al. 2002, Fernandez de la Mora, 2015). Tang (2016) has short-circuited this difficulty by isolating electrostatically both emitters, each with its own extractor electrode. Since Tang's purpose was to obtain primarily neutral particles, he has introduced an electric field in the neutralization region to drive the two charged clouds against each other. We have used a single grounded screen to isolate electrostatically one electrospray region from a neutralization region containing bipolar ions produced by a radioactive source (Fernandez de la Mora, 2015). In this way, the ES needle may be brought very close to the screen without any disruption from the neutralizing ions, as the strong electric field prevailing in the vicinity of the spraying capillary does not penetrate through the screen. Our study explored an alternative scenario where the screen was replaced by a small orifice perforated in a separating plate. Two problems arose: First, the spraying tip had to be brought fairly far from the orifice, resulting in substantial spray dilution. Otherwise, ES field leakage through the orifice and penetration of ions from the neutralization chamber destabilized the spray. The effectiveness of the screen approach suggests that the sprayed ions are efficiently propelled through the screen into the neutralization region by their own space charge, enabling a charge-reduction region completely free from electric fields. Space charge self-propulsion then appears to offer relatively large ion lifetimes, and is preferable to Tang's (2016) configuration (an electric field in the neutralization chamber), particularly when the objective is to produce primarily singly charged ions rather than neutrals. TSI's commercial *Advanced Aerosol Neutralizer 3088* isolates the spray region from a second neutralization chamber (containing bipolar ions produced by a soft X-ray source) with a metallic plate having a small orifice. This design opposes penetration of the ions into the ES chamber by passing a high-speed gas through the orifice from the ES chamber into the neutralization chamber, permitting on the one hand bringing the ES needle relatively close to the orifice, while also bringing the charged drops very quickly into the charge-reduction region, even before they have a chance to dry. Achieving a high jet speed, however, requires pressurizing the source chamber, which introduces some practical difficulties. In our own design with a small separation plate we found that the higher resulting jet speed limits the neutralization power relative to lower gas speed in the screen approach (Fernandez de la Mora, 2015). However, this limitation may be overcome with a neutralization chamber large enough for the jet speed to decay.

Given these various precedents, it seemed to us that the proven strategy of isolating with a metallic screen one spray region from another bipolar ion region should be equally effective in isolating two oppositely polarized sprays. Furthermore, space charge should in this case drive even more effectively each of the charged clouds from its original source, through the screen, into the oppositely charged cloud. Once two nearby oppositely polarized sprays are stabilized (with a screen or otherwise) an obvious advantage of this charge-reduction scheme is the great flexibility with which the anion and the cation may be controlled. For instance, by spraying the same salt in the two opposed polarities, only one anion and one cation would be combined (rather than 3 or more different species, as in conventional gas phase charge-reduction). Then, if the residence time in the charge reduction chamber were controlled to yield mainly singly charged particles, the simple one-parameter series of clusters $(B^-_n A^+_{n\pm 1})^{\pm 1}$ formed would extend to much larger n values than the currently accessible size range n= 0, 1. The viability of this approach will be demonstrated here.

Table 1: Ions and salts tested

Ions	Abbrev.	Composition	M_w	Salts
Tetrabutylammonium$^+$	C_4^+	$(C_4H_9)_4N^+$	242.47	C_4^+-TPB$^-$
Tetraheptylammonium$^+$	C_7^+	$(C_7H_{15})_4N^+$	410.80	$C_7^+Br^-$
Tetradodecylammonium$^+$	C_{12}^+	$(C_{12}H_{25})_4N^+$	691.34	$C_{12}^+Br^-$
Tetrahexadecylammonium$^+$	C_{16}^+	$(C_{16}H_{33})_4N^+$	915.77	$C_{16}^+Br^-$
bis(trifluoromethylsulphonyl)Imide$^-$	Im$^-$	$(CF_3SO_2)_2N^-$	280.14	$P_{6,6,6,14}^+Im^-$
1-Methyl-3-pentylimidazolium$^+$	MC_5I^+	$CH_3(C_3N_2H_3)C_5H_{11}^+$	153.24	$P_{6,6,6,14}^+FAP^-$
Tris(pentafluoroethyl)PF_3^-	FAP$^-$	$(C_2F_5)_3PF_3^-$	445.01	$MC_5I^+FAP^-$
Trihexyltetradecylphosphonium$^+$	$P_{6,6,6,14}^+$	$(C_6H_{13})_3(C_{14}H_{29})P^+$	511.91	EMI$^+$Methide$^-$
Br$^-$	Br$^-$	Br$^-$	79.904	
1-Ethyl-3-Methylimidazolium$^+$	EMI$^+$	$CH_3(C_3N_2H_3)C_2H_5^+$	111.17	
tris(trifluoromethylsulphonyl)Methide$^-$	Methide$^-$	$(CF_3SO_2)_3C^-$	411.2	
Tetraphenylborate$^-$	TPB$^-$	$(C_6H_5)_4B^-$	319.234	

2. Experimental

Sprayed solutions. The salts chosen are listed in the right column of Table 1. They combine the ions listed in the left column. Corresponding formulae and abbreviations are also given in the Table. The two salts including the FAP^- anion (Ignat'ev et al., 2005) and $P_{6,6,6,14}^+Im^-$ originated from Merck, but were obtained indirectly from generous colleagues. $C_7^+Br^-$ and $C_{12}^+Br^-$ were from Fluka, EMI$^+$Methide$^-$ from Covalent and $C_4^+TPB^-$ from Sigma.

The positive and negative sprays used exactly the same solution. $C_4^+TPB^-$ was dissolved in acetonitrile due to its poor solubility in ethanol. All other salts were dissolved in ethanol. Those that are liquid at room temperature ($P_{6,6,6,14}^+Im^-$, $P_{6,6,6,14}^+FAP^-$, $MC_5I^+FAP^-$, $EMI^+Methide^-$) were at 10^{-3} volumetric concentrations, and the solid salts at ~ 2 mM.

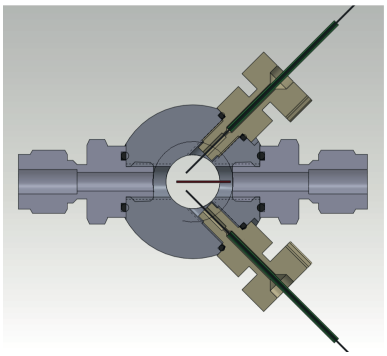

Figure 1. Scheme of the bipolar electrospray chamber with front and back windows; two gray connectors (PEEK) oriented at 90^o bringing in one positive and one negative capillary emitters and gas inlet (right) and outlet (left) connections. A stainless steel grid 30% transparent is symmetrically placed between the capillaries to decouple them electrostatically.

Bipolar ES chamber. Figure 1 sketches the chamber, commercialized by SEADM. It is structurally similar to other ES chambers previously used with a single capillary source, based on a cylindrical body with two windows at its bases, with gas inlet and outlet ports on the sides (Fernandez de la Mora, 2015, Figure 1). The new chamber combines these

prior elements with two rather than one liquid chromatography adaptor, enabling introducing two silica capillaries. The capillaries are coplanar with the inlet-outlet axis of the chamber, and are oriented symmetrically at ~ 45° with respect to that axis. As the capillaries are pulled from outside the chamber along their axes, the separation between their tips increases, decreasing their mutual electrostatic interaction. The capillaries are made out of silica with inner diameter of either of 75 or 170 μm, and outer diameters of 360 μm (Polymicro Technologies). Their emitting tips are manually pulled under a flame down to a closed cone, cut at the desired capillary tip opening size (30-40 μm), and finally sharpened to a conical tip by rotating them by hand about their axis, while the tip touches lightly a rotating polished flat alumina surface. A stainless steel screen 30% transparent (to light) placed at the plane of symmetry between the two capillaries was used in most experiments. The screen was supported on the gas inlet port. It could be displaced up and down, but its lower end was in most cases slightly downstream the point where the two capillaries intersect. Therefore, even when the two emitters were very close to each other, the two Taylor cones were out of direct sight. Under such conditions the two sprays were easily stabilized at all positions upstream of the point of intersection of the capillaries. We also examined briefly a scenario without screen, with the capillaries placed as far as possible from each other while being still visible through the window. The sprays were also stable in this configuration, each Taylor cone being barely influenced by changes in the voltage of the other.

DMA. Two different cylindrical DMAs of relatively high resolving power at particle diameters of 1 nm were used. One, dubbed the Halfmini, has inner and outer electrode radii R_1=4 mm; R_2=7mm, and an axial distance L=20 mm between the inlet and outlet slits (Fernandez de la Mora & Kozlowski, 2013). The other, referred to as a Herrmann DMA is a considerably lengthened (L=10 cm) modification of a DMA having R_1=4 mm, R_2=9 mm, and a wide laminarization trumpet. Shorter versions of the Hermann DMA have been widely used in scientific studies, though without a detailed characterization of its performance. This gap has been recently filled by Kangasluoma et al. (2016), who, however, report a resolving power much inferior to what had been previously shown in the literature (Ku et al. 2004a, b and 2009; Saucy et al. 2004; Gamero et al., 2000 a, b, c). Most of the exploratory work on the cluster source was done with the Halfmini DMA. The Herrmann DMA was used only in a few experiments (described at the end of the article) meant to characterize its resolving power.

A flow rate q_i of approximately 2 Lit/min (controlled by a flowmeter) of filtered and dried air passes through the bipolar electrospray chamber, entraining the electrosprayed clusters into the polydisperse aerosol inlet to the DMAs. The DMA-selected monodisperse aerosol is captured by an unusually fast (<100 ms response time) and sensitive (0.12 fA noise) Faraday cup electrometer commercialized by SEADM (Fernandez de la Mora et al, 2016), which measures the current I carried by the sampled gas. Its flow rate q_o is not controlled, but is automatically equal to q_i because the sheath gas flow circuit operates in closed loop, with a refrigeration system and a HEPA filter following the blower. The sheath gas flow rate Q was controlled by fixing the speed of rotation of the blower, but was not directly measured. Instead, Q is determined according to relation (1) (Knutson and Whitby, 1975) from the voltage V_{C7+} at the center of the most mobile peak appearing in a $I(V_{DMA})$ spectrum when electrospraying $C_7^+Br^-$:

$$Q = \frac{2\pi LZV}{ln(R_2 / R_1)}. \qquad (1)$$

Z is the electrical mobility under ambient conditions of the C_7^+ ion used as a mobility standard (Z_{C7+}=0.971 cm^2/V/s, according to Ude and Fernandez de la Mora, 2005).

Raw mobility spectra were obtained by fixing all flow rates and the setting of the electrospray source, sweeping the voltage V_{DMA} of the inner electrode while grounding the outer electrode, and recording (in a computer, with the help of a data acquisition card) the aerosol current collected as a function of V_{DMA}. The high voltage power supply used (Applied Kilovolts, ±10 kV, 30 ms response time from +10 to -10 kV) is bipolar and can go continuously through zero (Figure 2a), so bipolar spectra were taken as single data files. In Figure 2a V_{DMA} is negative for the positive ions and positive for the negative ions. The electrometer is an inverting amplifier giving a negative signal for positive ions. In order to save figure space, the negative currents will be inverted in subsequent figures (Figure 2b), as if the detector were measuring ion concentration.

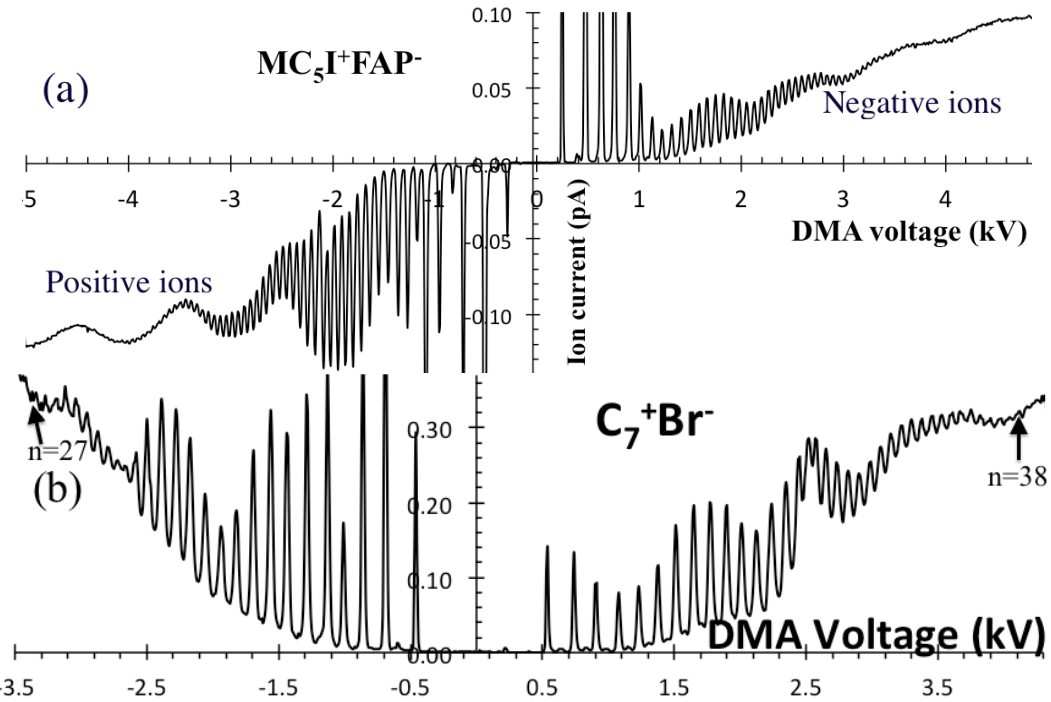

Figure 2: Bipolar spectra obtained when spraying (a) $MC_5I^+FAP^-$ and (b) $C_7^+Br^-$, both dominated by a resolvable series of singly charged clusters $A^+_nB^-_{n\pm1}$. The original spectrum format (a) is compacted in (b) by using absolute values of the current.

3. Results

3.1 Dominant production of singly charged clusters.

Figure 2a shows the full raw spectrum for $MC_5I^+FAP^-$. Both the negative and positive domains resolve over 40 major peaks associated to singly charged ions. This $MC_5I^+FAP^-$ spectrum is taken at limited resolution (Q~605 Lit/min) in order to extend the size range and exhibit the transition from individually resolved peaks to just their envelope. Each of the broad modulations seen in the envelope is associated to the original charge state of the clusters prior to charge reduction (Gamero-Castaño and Fernandez de la Mora,

2000a). Figure 2b is for $C_7^+Br^-$, and is taken at higher resolving power. The negative spectrum resolves 36 major peaks associated to singly charged ions, including a weak peak (~220 Volt) of singularly high mobility associated to Br^-. In addition to the dominant series of ions, much weaker peaks are resolvable in the space between major peaks. Only the monomer A^+ and the dimer $(A^+B^-)A^+$ are isolated in conventional unipolar electrospray spectra of alcohol solutions of $C_7^+Br^-$. The trimer $(A^+B^-)_2A^+$ typically emerges over a substantial background of multiply charged species, and the tetramer $(A^+B^-)_3A^+$ is almost invariably undetectable, overwhelmed by the background of multiply charged particles. The radical shift observed here from the usual undetectable singly charged ions beyond the trimer, into their complete dominance of the spectrum, shows that the charge-reduction process is successful in removing all but the lowest charge states.

The positive spectrum for $C_7^+Br^-$ is similarly dominated by singly charged species, although it does not in this case show as many clearly defined peaks as the negative series. The number of peaks that may be distinguished depends considerably on the circumstances of the measurement, especially on the stability of both sprays. This is inevitable given that the largest clusters have mobilities very close to those of their neighbors, so the ripple associated to each individual peak rises only a few percent above the average signal. At high enough n in the $A^+_nB^-_{n\pm1}$ series, this ripple is no longer observable because of the limited resolution of the Halfmini DMA used. When the neighboring peaks are still resolvable but a slight unsteadiness of the spray current becomes comparable in magnitude to the ripple between peaks, the peaks also become unresolvable, as in the positive spectrum in Figure 2b past n=27. While a high stability of both sprays is absolutely essential to see the large number of cluster reported in Figure 2, numerous peaks can nonetheless be observed under less exacting conditions.

A similar pattern of dominantly singly charged clusters has ben observed with all the salts tested (Table 1, last column). The salt for which the largest number of cluster peaks has been resolved is $MC_5I^+FAP^-$ (n_{max}=43). The corresponding bipolar spectra are shown in Figure 3 at higher DMA resolving power than in Figure 2a. $C_{16}^+Br^-$ was also tested but did not produce an extended clean cluster series (Auxiliary Figure A2), probably because its minimal solubility in ethanol.

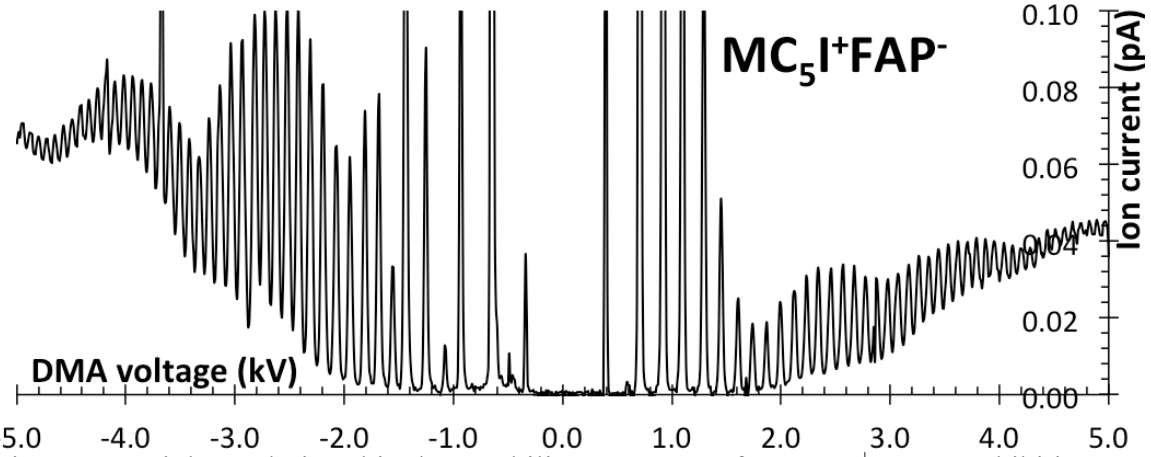

Figure 3: High-resolution bipolar mobility spectrum for $MC_5I^+FAP^-$, exhibiting 43 resolvable peaks in each polarity.

A surprising finding was that some salts produce wider ion mobility peaks than others. This was evident for $C_{12}^{+}Br^{-}$ and for the two salts including the Trihexyltetradecylphosphonium cation. This peculiar broadening cannot be due to the DMA, as it happened at exactly the same DMA setting at which other salts gave narrower peaks. Perhaps some clusters have variable shapes and are accordingly not ideal mobility standard. This structural floppiness is well documented in protein ions. It would not be so surprising in the case of solid salts such as $C_{12}^{+}Br^{-}$ having very long alkyl branches, which could interfere with the formation of the structure having minimal energy. In the case of the phosphonium ionic liquids, however, assuming that the clusters are also liquid-like, one would expect the cluster to sample all possible shapes millions of times during the DMA measurement, resulting in a unique mobility. Another possible cause of broadening is the presence of contaminants in the salt. This has been documented in mobility mass-spectrometry measurements with large tetra-alkylammonium salts (May et al. 2014). It is also evident in some of our measurements. For instance, one sample tried of $C_4^{+}TPB^{-}$ (Figure A3 in Auxiliary Information) gives very sharp peaks, many of which are from impurities. The clusters from the dominant series may be resolved from the impurities (up to a point), revealing *FWHM* as small as 0.02.

3.2 Size range spanned by mobility-resolvable bipolar standards

The various spectra have been so far shown in terms of the DMA voltage, the key quantity governing diffusion broadening and hence limiting resolving power. In order to convert voltage to particle mobility and infer the mobility diameter we have run back-to-back spectra with $C_7^{+}Br^{-}$, and the two FAP^{-} salts, from which we measure the voltage for the most mobile ion and infer the mobility/voltage calibration data collected in Table 2. The flow rate of sheath gas given by equation (1) was 830 lit/min. It is noteworthy that, in spite of their large masses, the FAP^{-} and Im^{-} anions are rather compact, with mobilities not far from the polarization limit (~2 $cm^2/V/s$).

Table 2: Relation between classification voltage and mobility *Z* for four of the ions used.

Ion	*V* (Volt)	*1/Z* ($Vs\ cm^{-2}$)
C_7^{+}	633.7	1.03
FAP^{-}	395	0.642
MC_5I^{+}	350	0.569
$P_{6,6,6,14}^{+}$	675	1.097
Im^{-}	355	0.577
C_{12}^{+}		1.401
Br^{-}		0.494

The tabulated values have not been obtained precisely enough to be interchangeable with the common C_7^{+} standard, but rather to determine approximately the sizes of the large particles for which pure clusters are resolvable by mobility alone. For example, in Figure 3, the largest cluster resolved appears at about 4.9 kV, with $1/Z$=1.03*4.9/0.6337 $Vs\ cm^{-2}$

= 7.96 Vs cm^{-2}. The corresponding free-molecule mobility diameter $d_Z=(k/Z)^{1/2}$ is 4.03 nm when taking k=2.04 cm^2/V/s/nm^2.

3.3 Use of the bipolar ES source for DMA resolution measurements

The development of nanoDMAs with high resolving powers would not have been possible without the availability of molecular standards. However, as we have attempted to extend the range of these instruments beyond their original domain (< 10 nm) to 30 nm and beyond, a number of causes conspire to either limit DMA resolving power or preclude its measurement. Longer DMAs classify small ion standards at modest voltages, at which diffusion broadening results in *FWHM* typically > 0.03. Although in an ideal DMA at fixed flow conditions one would expect that peak width would continue decreasing as particle size increases, the lack of larger size standards has precluded confirming this point. Furthermore, as the DMA length increases to accommodate larger particles, it is harder to achieve good electrode centering, particularly in the aerodynamically favorable Reischl (1991) geometry, where the central electrode is supported only on the downstream end. While long DMAs may support their inner electrode on both ends and also have aerodynamically favorable sheath gas inlets, the likelihood of turbulent transition also increases with increased instrument length. As a result, in our recent work with proteins and viral particles, we have been unable to ascertain if the finite peak widths found were intrinsic to these particles, or were rather due to non-ideal DMA response. In fact, the maximum resolving power so far reported for the *long* (2 cm) Halfmini DMA is in the range 30-40, and is limited by the previously available size standards. As seen in Figures 2-4, resolvable peaks are now generated by the bipolar source at mobilities about 10 fold those previously available, enabling in principle a reduction by $10^{1/2}$ (=3.16) the diffusion-limited peak width.

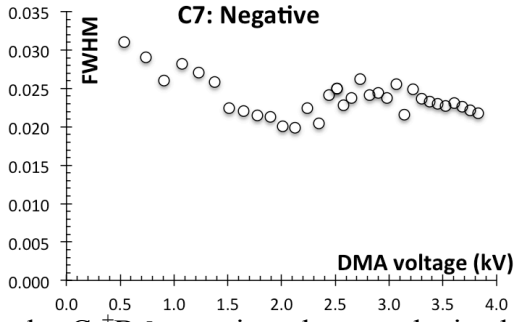

Figure 4: Peak width for the $C_7^+Br^-$ negative clusters obtained by Gaussian fitting the spectrum of Figure 2b.

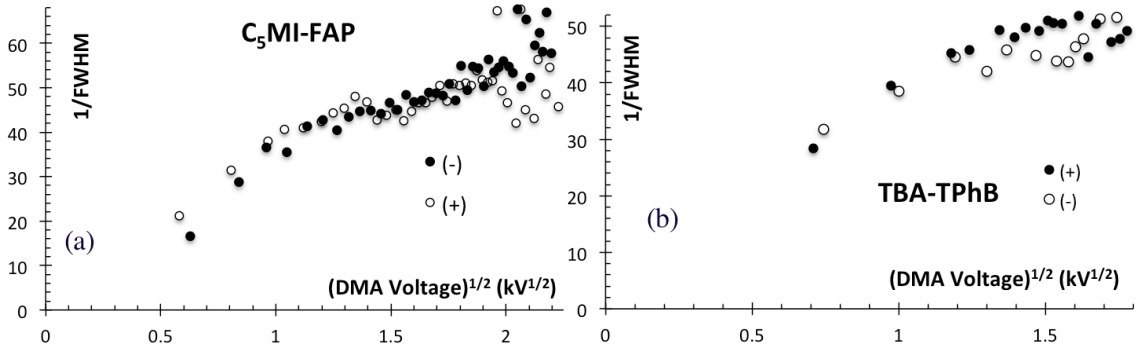

Figure 5: Resolution (1/*FWHM)* for the Halfmini DMA challenged with $MC_5I^+FAP^-$ (a) and $C_4^+TPB^-$ clusters (b), demonstrating resolving powers >50 with sufficiently large particles.

HalfMini DMA. We have determined peak widths by fitting the spectra previously presented to a linear combination of Gaussians. Figure 4 plots *FWHM* for negative $C_7^+Br^-$ clusters in the spectrum of Figure 2b. Their width decreases initially with DMA voltage, but exhibits an unnatural transition above 2 kV. This is surely an artifact following from incomplete separation of the peaks above that voltage. Indeed, the Gaussian inversion has been performed assuming the complete absence of a broad background of impurities under the partially resolved peaks, which artificially increases their height and the inferred width. In spite of this limitation, the Figure demonstrates a resolving power greater than 50, unprecedented for a DMA whose length over gap ratio $L/(R_2-R_1) = 6.67$ exceeds considerably the ideal ratio of 1.
The spectra of $C_4^+TPB^-$ (Figure A4) have been analyzed in Figure 5b more carefully than those of $C_7^+Br^-$. In this case we have included resolvable impurity ions in the Gaussian fitting, so as to remove their interference. As an additional precaution, the widths of secondary peaks have not been used to determine resolving power. This more thorough analysis confirms that the resolution exceeds 50. Figure 5 plots the resolution versus $V_{DMA}^{1/2}$ because the ideal diffusion broadened resolution is a straight line through the origin, facilitating a visual extrapolation of the data. No comparison with theory is provided in that figure because the performance always falls below the pure diffusion limit. Since the level of peak interference and the noise in inferred resolution become substantial as the resolving power reaches 50, it would be dangerous to extrapolate this trend. The cleaner mobility spectra obtained with $MC_5I^+FAP^-$ (Figure 3) have resulted in the peak width measurements of Figure 5a, demonstrating for the first time that this DMA has regimes reaching a resolution of 52-54. Although peak interference precludes reliable resolution inferences beyond this value, the slope of the curve shows no sign of saturation. The resolving power of this DMA is clearly better than 52, but the bipolar clusters available are not capable of measuring it beyond this value. While changes in the flow rates over the very large range of values open to this instrument may lead to drastic variations over this performance, this limited result under even one condition provides complete assurance that the concentricity of the instrument is not a limiting feature.

Herrmann DMA. This is the first prototype ever built of a Herrmann DMA with an axial length as large as 10 cm. It was modified from a shorter Herrmann DMA to study viral particles over the size range up to 60 nm, a development still in progress. Given the wide size range of this DMA it had previously not been possible with conventional cluster standards to establish if its resolving power exceeded even 18. This ambiguity has frustrated our goal of separating virus particles with a resolution exceeding 30. Given the limited available information on the intrinsic mobility peak width for viruses following electrospray charge reduction, it has remained unclear if one needs to focus on improving the DMA, the charge reduction process, the solution cleaning protocol, etc.
The new bipolar source has greatly clarified these doubts. Figure 6 shows a bipolar spectrum for an electrospray of the $EMI^+Methide^-$ ionic liquid, including 25 resolved ions in the positive spectrum. The corresponding resolving power is shown in Figure 7,

showing a resolving power reaching up to 33, with no indication of saturation with increasing particle size.

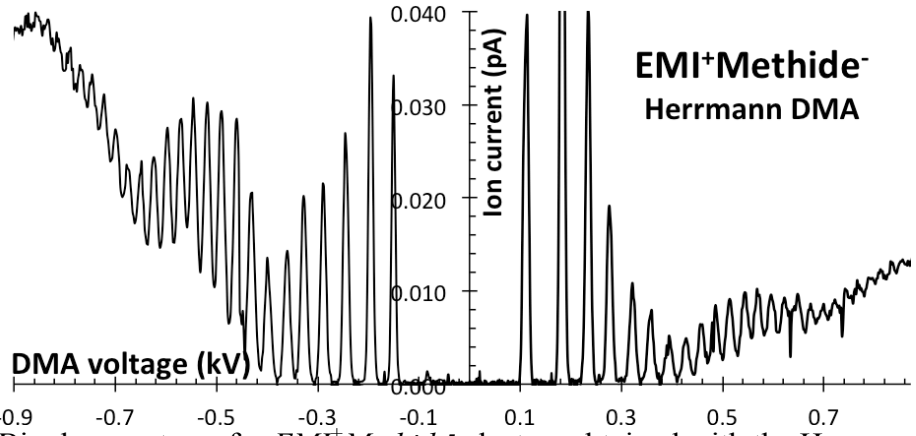

Figure 6: Bipolar spectrum for *EMI*$^{+}$*Methide*$^{-}$ clusters obtained with the Herrmann DMA

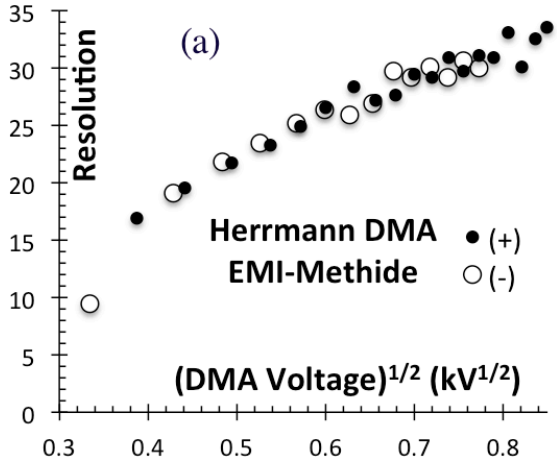

Figure 7: Resolution for the Hermann DMA with *EMI*$^{+}$*Methide*$^{-}$, limited by diffusion in the DMA.

4. Conclusions

Electrostatic isolation with a metallic grid of two oppositely polarized electrosprays enables their stabilization even when the emitting tips are very close to each other. Interaction of the two oppositely charged sprays then leads to efficient charge reduction, resulting in a bipolar aerosol dominated by singly charged clusters.

This behavior is as expected based on prior experience with a charge-reduction system where a metallic grid separated electrostatically the spray region from a bipolar ion region. One substantial advantage of the bipolar electrospray is that, when the same salt solution is sprayed from both capillaries, the clusters formed are members of the simple series of pure species $(A_n^+B_{n\pm l}^-)^{\pm l}$, defined by the single parameter n. Many members of this series can be resolved by mobility alone, offering a simple means to provide an aerosol of nanoparticles with essentially pure composition. By classification with a Halfmini DMA the cluster size may be changed from a single molecular ion up to 4 nm. Use of a DMA with a superior resolving power would extend this maximum resolvable

cluster size. We have also attempted to increase the maximal resolvable size by operating with salts composed of unusually large anions and cations. The few tested here involving C_{16}^+, C_{12}^+, and the $P_{6,6,6,14}^+$ phosphonium cation have not been successful, perhaps due to the lack of either a rigid structure or sufficient sample purity. We trust this strategy will be fruitful if more systematically pursued.

The $MC_5I^+FAP^-$ salt is the one so far having yielded the narrowest mobility distributions, with over 43 positive clusters resolvable reaching particle sizes up to 4 nm.

These standards have been exploited here to characterize two nanoDMAs designed to go beyond the 10 nm size range previously characterizable with available 1 nm size standards. The 2 cm long Halfmini DMA has been seen to achieve resolving powers beyond 50, considerably larger than previously considered possible. The 10 cm Herrmann DMA designed for viral particle analysis has a resolving power of at least 33, which continues increasing monotonically with particle size.

Acknowledgment. We thank Mr. Mario Amo-Gonzalez of SEADM for his valuable inputs in the design of the bipolar source chamber. We are indebted to Prof. Michel Attoui (Paris) and Luis J. Perez-Lorenzo (Yale) for numerous contributions to the experimental setup used to characterize the bipolar chamber.

Conflict of interest statement. Juan Fernandez de la Mora declares a personal interest in the company SEADM commercializing the DMA, the electrometer and the bipolar electrospray source used in this work.

References

Attoui, A. Paragano, M., Cuevas, J., Fernandez de la Mora,J. 2013 Tandem DMA generation of strictly monomobile 1-3.5 nm particle standards, Aerosol Science and Technology, **47(**5)**.** 499-511

Borra, J. P., Camelot, D., Chou, K.-L., Kooyman, P. J., Marijnissen, J. C. M., and Scarlett, B. (1999) Bipolar Coagulation For Powder Production : Micro-Mixing Inside Droplets," *J. Aerosol Sci.*, 30(7), 945–958.

Fenn, J. B.; Mann, M.; Meng, C. K.; Wong, S. F.; Whitehouse, C. M. (1989) Science, 246, 64−71.

Fernandez de la Mora, J. (2011) Heterogeneous nucleation with finite activation energy and perfect wetting: Capillary theory versus experiments with nanometer particles, and extrapolations on the smallest detectable nucleus, Aerosol Sci. Tech. **45**(4), 543-554

Fernandez de la Mora, J., and J. Kozlowski (2013) Hand-held differential mobility analyzers of high resolution for 1-30 nm particles: Design and fabrication considerations. J. Aerosol Sci. (57) 45-53

Fernandez de la Mora, J. (2015) High-Resolution Mobility Analysis of Charge-Reduced Electrosprayed Protein Ions, Anal. Chem., 87, 3729−3735

Fernandez de la Mora, J., Perez-Lorenzo, L. J., Arranz, G., Amo-Gonzalez, M., Burtscher, H. (2016) Fast high-resolution nanoDMA measurements with a 25 ms response time electrometer, submitted to Aerosol Sci. & Tech.

Gamero-Castaño, M., Fernandez de la Mora, J. (2000 a) Modulations in the abundance of salt clusters in electrosprays, Anal. Chem., **72**, 1426-1429

Gamero-Castaño, M., J. Fernandez de la Mora, J. (2000 b), Mechanisms of electrospray

ionization of singly and multiply charged salt clusters, Anal. Chimica Acta, **406**, 67-91
Gamero-Castaño, M., J. Fernandez de la Mora, J. (2000 c) Kinetics of small ion evaporation from the charge and size distributions of multiply charged electrospray clusters, J. Mass Spectrometry, **35**, 790-803
Gamero-Castaño, M. and Fernandez de la Mora (2000d) A condensation nucleus counter (CNC) sensitive to singly charged subnanometer particles; J. Aerosol Sci., **31**, 757-772
Ignat'ev, N.V., Welz-Biermann, U., Kucheryna, A., Bissky, G. (2005) New ionic liquids with tris(perfluoroalkyl)trifluorophosphate (FAP) anions, Journal of Fluorine Chemistry, 126(8) 1150–1159
Jiang, J. K., Zhao, J., Chen, M. D., Eisele, F. L., Scheckman, J., Williams, B. J., McMurry, P. H.(2011). First measurements of neutral atmospheric clusterand 1–2 nm particle number size distributions during nucleation events. Aerosol Science and Technology, 45(4), pp ii-v.
Kane, D., Daly, G. M., El-Shall, S. (1995) J. Phys. Chem. 99, 7867
Kane, D., El-Shall, S. (1996) Chem. Phys. Lett. 259, 482
Kangasluoma, M. Attoui, F. Korhonen, L. Ahonen, E. Siivola, and T. Petäjä (2016) Characterization of a Herrmann-type high-resolution differential mobility analyzer, Aerosol Sci. & Tech. 50(3), 222-229
Kangasluoma, J., Samodurov, A., Attoui, M., Franchin, A., Junninen, H. Korhonen, F., Kurtén, T., Vehkamäki, H., Sipilä, M., Lehtipalo, K., Worsnop, D. R., Petäjä, T., Kulmala, M. (2016) Heterogeneous Nucleation onto Ions and Neutralized Ions: Insights into Sign-Preference, J. Phys. Chem. C, 120, 7444−7450
Kaufman, S. L.; Skogen, J. W.; Dorman, F. D.; Zarrin, F.; Lewis, K. C. (1996) Anal. Chem., 68, 1895−1904.
Kaufman, S.L., Dorman, F.D. (2008) Sucrose clusters exhibiting a magic number in dilute aqueous solutions, Langmuir 24(18) 9979-9982
Knutson, E. O., and K. T. Whitby (1975a) Aerosol Classification by Electric Mobility: Apparatus Theory and Applications, J. Aerosol Sci. 6:443-451.
Ku, B. K., Fernandez de la Mora, J., Saucy, D.A, Alexander, J. N. (2004a), Mass distribution measurement of water-insoluble polymers by charge-reduced electrospray mobility analysis, Analytical Chemistry, **76,** 814-822
Ku, B. K., Fernandez de la Mora, J. (2004b) Cluster ion formation in electrosprays of acetonitrile seeded with ionic liquids, J. Phys. Chem. B, **108**, 14915-14923
Ku, B. K., Fernandez de la Mora, J. (2009) Relation between Electrical Mobility, Mass, and Size for Nanodrops 1-6.5 nm in Diameter in Air, Aerosol Sci. & Techn., **43 (**3), 241-249
Lenggoro I.W., Xia B., Okuyama K., Fernandez de la Mora J. (2002) Sizing of colloidal nanoparticles by electrospray and differential mobility analyzer methods. Langmuir 18(12):4584‑4591
May, J. C., C. R. Goodwin, N. M. Lareau, K. L. Leaptrot, C. B. Morris, R. T. Kurulugama, A. Mordehai, C. Klein, W. Barry, E. Darland, G. Overney, K. Imatani, G. C. Stafford, J. C. Fjeldsted, J. A. McLean, Conformational Ordering of Biomolecules in the Gas Phase: Nitrogen Collision Cross Sections Measured on a Prototype High Resolution Drift Tube Ion Mobility-Mass Spectrometer, Anal. Chem. 2014, 86, 2107−2116

Reid, G. E.; Wells, J. M.; Badman, E. R.; McLuckey, S. A. (2003) Int. J. Mass Spectrom. 222, 243−258.

Reischl, G. P. (1991) Measurement of Ambient Aerosols by the DifferentialMobility Analyzer Method: Concepts and Realization criteria for the SizeRange between 2 and 500 nm.Aerosol Sci. Technol.14: 5-24

Rosell, J., Loscertales, I. G., Bingham, D., Fernández de la Mora, J. (1996) Sizing nanoparticles and ions with a short differential mobility analyzer, J. Aerosol Sci., 27, 695-719.

Saucy, D., Ude, S., Lenggoro, W., Fernandez de la Mora, J. (2004) Mass analysis of water-soluble polymers by mobility measurement of charge-reduced electrosprays, Anal. Chem. 76,1045-1053

Steiner, G., Franchin, A., Kangasluoma, J., Kerminen, V-M., Kulmala, M. and Petäjä, T. (2017) Production of neutral molecular clusters by (controlled) neutralization of mobility standards, Aerosol Sci. & Tech., under review.

Stolzenburg, M.R. (1988). An Ultrafine Aerosol Size Distribution Measuring System. Ph.D. Thesis, University of Minnesota: Minneapolis, MN.

Tammet, H.F. (1970) The Aspiration Method for the Determination of Atmospheric-ion Spectra. Israel Program for Scientific Translations. Jerusalem. The original work in Russian was published in 1967.

Tang, J. (2016) Application of Electrospraysfor Nanomaterial Deposition and Synthesis for Energy Conversion and Storage Devices, Ph.D. Thesis, Yale University

Tang, K., Gomez, A. (1995) Generation of Monodisperse Water Droplets from Electrosprays in a Corona-Assisted Cone-Jet Mode, J. Colloid Interface Sci., 175(2) 326–332

Ude, S., Fernández de la Mora, J. (2005) Molecular monodisperse mobility and mass standards from Electrosprays of tetra-alkyl ammonium halides, J. Aerosol Sci, **36** (10) 1224-1237.

Winkler, P. M., Vrtala, A., Steiner, G., Wimmer, D., Vehkamäki, H., Lehtinen, K. E. J., Reischl, G. P., Kulmala, M., Wagner, P. E. (2012) Quantitative characterization of critical nanoclusters nucleated on large single molecules", Phys. Rev. Lett. 108, 085701.

You, R.; Li, M.; Guha, S.; Mulholland, G. W.; Zachariah, M. R. (2014) Bionanoparticles as Candidate Reference Materials for Mobility Analysis of Nanoparticles, Anal. Chem. 86, 6836−6842